^{1}H-Detected Multinuclear NMR Experiments for the Measurement of Small Heteronuclear Coupling Constants in Transition Metal Complexes

Gottfried Otting,[†] Barbara A. Messerle,*[,‡] and Linnea P. Soler[‡]

Contribution from the Department of Medical Biochemistry and Biophysics, Karolinska Institute, S-171 77 Stockholm, Sweden, and Department of Organic Chemistry, University of Sydney, Sydney NSW 2006, Australia

Received September 24, 1996[⊗]

Abstract: The scalar coupling constants between protons, nitrogens, and phosphorus in the metal complex chloro(triphenylphosphine)bis[bis(1-pyrazolyl)methane]ruthenium(II) chloride, $[RuCl(PPh_3)(BPM)_2]^+Cl^-$ (**1**), were measured with a set of specially adapted NMR experiments. The absolute sign of the coupling constants was determined by relating the signs of the measured couplings to that of a one-bond proton−carbon coupling constant. A complete set of coupling constants >|0.4| Hz was obtained with use of a single sample with 99% ^{15}N-labeled bis-pyrazolyl ligands. The data show that the two-bond ^{15}N−^{15}N and ^{31}P−^{15}N couplings across the metal center are significantly larger, if the two metal-ligating atoms are trans rather than cis with respect to one another. Furthermore, all trans couplings $^2J_{PN}$ and $^2J_{NN}$ are positive, while the corresponding cis couplings are negative or too small to be measured. The conformation dependence of the scalar coupling constants supports the rapid structural characterization of catalytically active organometallic complexes by NMR spectroscopy. The proposed set of NMR experiments includes HSQC experiments with small flip angles, a quantitative long-range ^{15}N−^{15}N correlation experiment, and DQ/ZQ experiments for the determination of the sign and size of J_{NN} and J_{PN} coupling constants in linear spin systems.

Introduction

Organometallic complexes like the tris(1-pyrazolyl)borate complexes of Ir,[1] Rh,[2] and Re[3] are reactive species that can insert into C−H bonds. Many different ligand configurations are conceivable to modify the reactivity and specificity of these metal complexes. NMR provides powerful tools for a rapid analysis of the stereochemical structure of these reactive complexes. The most important NMR parameters are the nuclear Overhauser effect and scalar coupling constants. For example, it has been established for a number of metal phosphine complexes that the relative sign and magnitude of the $^2J(^{31}P,^{31}P)$ and $^2J(^1H,^{31}P)$ coupling constants across the metal center is characteristic of the geometry of the metal coordination, e.g. $^2J_{P-M-P}$(trans) > $^2J_{P-M-P}$(cis).[4,5] A $^2J_{NN}$ coupling constant of 4.3 Hz was reported for a non-octahedral iron complex,[6] indicating that $^2J_{NN}$ couplings should be generally measurable. In the present work, a complete set of magnitudes and signs of $^2J_{NN}$ and $^3J_{NN}$ coupling constants across a metal center was determined. A series of improved NMR experiments for the measurement of magnitude and sign of J_{HN}, J_{NN}, J_{HP}, and J_{PN} coupling constants is presented.

The compound investigated was chloro(triphenylphosphine)bis[bis(1-pyrazolyl)methane]ruthenium(II) chloride, $[RuCl(PPh_3)(BPM)_2]^+Cl^-$ (1).[7] This complex is chemically unreactive

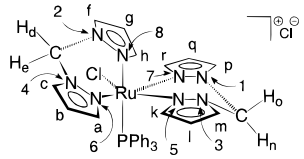

(1)

and was chosen as a model system to establish an NMR analysis protocol, since the bis(1-pyrazolyl)methane ligands are closely related to the tris(1-pyrazolyl)methane ligand studied in detail previously.[8] The compound was fully and uniformly enriched with ^{15}N to facilitate the determination of J_{NN} coupling constants. Ruthenium was used at natural isotopic abundance.

The experiments used for the measurement of signs and sizes of the J_{HN}, J_{NN}, and J_{CN} coupling constants in tris(1-pyrazolyl)-methane[8] proved to be less efficient with the more complex and fully ^{15}N-labeled compound **1**. The present set of experiments is based on the HSQC[9] rather than the HMQC[10] experiment. In addition, novel pulse sequences were developed specifically for the measurement of small heteronuclear coupling constants across the metal center in organometallic complexes. The experiments are straightforward to set up, and the results easy to interpret. In particular, all experiments encoding the coupling constants in E. COSY type multiplet patterns yield a positive tilt of the multiplet fine structure if the sign of the couplings is the same in the F_1 and F_2 dimension; a negative

[†] Karolinska Institute.
[‡] University of Sydney.
[⊗] Abstract published in *Advance ACS Abstracts,* April 15, 1997.

(1) Tanke, R. S.; Crabtree, R. H. *Inorg. Chem.* **1989**, *28*, 3444−3447.
(2) Ghosh, C. K.; Graham, W. A. *J. Am. Chem. Soc.* **1987**, *109*, 4726−4727.
(3) Brown, S. N.; Mayer, J. M. *J. Am. Chem. Soc.* **1994**, *116*, 2219−2220.
(4) Moore, D. S.; Robinson, S. D. *Chem. Soc. Rev.* **1983**, *12*, 415−452. Kaesz, H. D.; Saillant, R. B. *Chem. Rev.* **1972**, *72*, 231−281. Baker, M. V.; Field, L. D. *Inorg. Chem.* **1987**, *26*, 2010−2011.
(5) Bampos, N.; Field, L. D.; Messerle, B. A. *Organometallics* **1993**, *12*, 2529−2535.
(6) Butler, A. R.; Glidewell, C.; Hyde, A. R.; McGinnis, J. *Polyhedron* **1984**, *3*, 1165−1167.
(7) Field, L. D.; Messerle, B. A.; Soler, L. P.; Buys, I.; Hambley, T. W. *J. Chem. Soc., Dalton Trans.* Submitted for publication.
(8) Otting, G.; Messerle, B. A.; Soler, L. P. *J. Am. Chem. Soc.* **1996**, *118*, 5096−5102.
(9) Bodenhausen, G.; Ruben, D. J. *Chem. Phys. Lett.* **1980**, *69*, 185−189.
(10) Bax, A.; Griffey, R. H.; Hawkins, B. L. *J. Magn. Reson.* **1983**, *55*, 301−315.

S0002-7863(96)03346-X CCC: $14.00

tilt arises if the sign of the couplings is opposite in the F_1 and F_2 dimension. In addition, DQ/ZQ experiments are shown to yield the magnitudes, as well as the signs, of the coupling constants in linear three-spin systems involving couplings across the metal center.

Results

Resonance Assignments. The ^{1}H NMR spectrum of **1** was assigned from a NOESY spectrum recorded with a 1.6 s mixing time. The ^{13}C NMR spectrum was assigned through one-bond correlations with the protons in a ^{13}C-HMQC experiment. The ^{15}N signals were assigned to the individual pyrazolyl groups by the observation of ^{15}N−^{1}H cross peaks with all three protons within each pyazolyl spin system in long-range ^{15}N-HSQC experiments recorded with a 71-ms INEPT delay and a semiselective 180°(^{15}N) pulse inverting either the four low-field or the four high-field ^{15}N resonances (see below). The two ^{15}N resonances within the same pyrazolyl group were distinguished by the one-bond ^{13}C/^{12}C isotope effect on the ^{15}N chemical shift measured in a ^{15}N-HMQC experiment with ^{13}C half-filter.[8] The experiment showed >2-Hz upfield shifts for the nitrogen resonances 1−4 in the cross peaks N_4−H_c, N_2−H_f, N_1−H_p, and N_3−H_m, if the neighboring carbon isotope was ^{13}C instead of ^{12}C. The two-bond isotope effects measured from the cross peaks N_4−H_b, N_2−H_g, N_1−H_q, and N_3−H_l were all smaller than 1 Hz. Furthermore, the coupling constants $^1J_{CN}$ between the aromatic ^{13}C and the ^{15}N nuclei N_1 to N_4 were measured to be between about 12 and 14 Hz, while the $^2J_{CN}$ coupling constants measured between the ^{13}C spins at positions b, g, q, and l with the ^{15}N nuclei N_1 to N_4 were about 3−4 Hz. These data agree perfectly with the values measured in tris(1-pyrazolyl)methane for the ^{15}N nuclei bound to the aliphatic CH group.[8] The four resonances to highest field in the ^{15}N NMR spectrum of **1** are thus from the nitrogens bound to the methylene groups (N_1 to N_4), while the four low-field signals are from the metal coordinating nitrogens (N_5 to N_8).

Measurement of ^{1}H−^{15}N Coupling Constants. Most J_{HN} couplings in **1** are conveniently measured from a ^{15}N-HSQC-36N experiment. The pulse sequence is shown in Figure 1A. The desired magnetization at the end of the INEPT delay is proton magnetization antiphase with respect to a single ^{15}N spin, or H_xN_z in the product operator notation of Sørensen et al.[11] Since all J_{HN} couplings in **1** are small, a relatively long delay is required during which ^{1}H− ^{1}H and ^{1}H−^{15}N couplings to more than one ^{15}N spin could evolve to a significant extent. In particular, undesired doubly antiphase terms like $H_yN_{az}N_{bz}$ could be generated due to the similar magnitudes of the $^2J_{HN}$ and $^3J_{HN}$ coupling constants in the pyrazolyl rings. To avoid such loss of magnetization, half of the J_{HN} couplings were refocused by the use of a semiselective ^{15}N inversion pulse (Figure 1A), which inverted either the ^{15}N resonances of N_1, N_2, N_3, and N_4 or the ^{15}N resonances of N_5, N_6, N_7, and N_8 (see Experimental Section). The resulting spectra each contained only cross peaks with one of the two groups of nitrogens, so that two spectra with different frequency offsets of the selective pulse had to be recorded to obtain all ^{15}N−^{1}H correlations. This strategy did not result in longer experimental times, since the sensitivity in each of the experiments was much improved compared to a nonselective experiment, and a narrower spectral width in the F_1 dimension could be used.

The ^{1}H−^{1}H couplings in **1** are all less than 3 Hz, except for the coupling between the geminal protons of the methylene groups, which is about 14 Hz. To avoid the presence of antiphase coherence between the geminal methylene protons by the end of the delay Δ in the sequence of Figure 1A, Δ was set to 1/14 s. In molecules with a larger spread of J_{HH} coupling constants, the nonselective 180°(^{1}H) pulse in the middle of the delay could be replaced by a selective ^{1}H refocusing pulse to refocus the most disturbing J_{HH} couplings (Figure 1A).

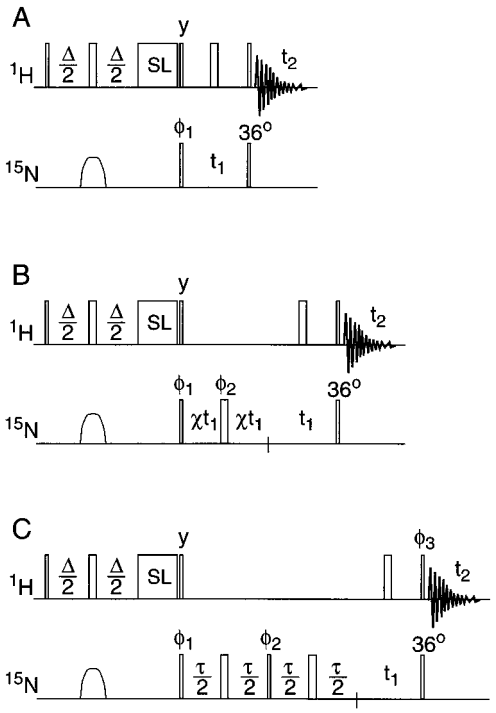

Figure 1. Pulse sequences for the measurement of ^{1}H−^{15}N coupling constants. Narrow and wide bars denote 90° and 180° pulses, respectively. Selective pulses are identified by smooth shapes. In all experiments, $\Delta = 1/(2J_{HN})$, SL denotes a spin-lock pulse of 1-ms duration, and the last ^{15}N pulse is a 36° pulse. Here and in all subsequent figures, all pulses are applied along the *x*-axis unless indicated otherwise. The first ^{15}N pulse is a semiselective shaped pulse inverting a subset of the ^{15}N resonances. (A) ^{15}N-HSQC-36N. The experiment yields E. COSY type multiplet patterns with J_{NN} in F_1 and J_{HN} in the F_2 dimension. Furthermore, passive couplings with ^{31}P are observed in both dimensions. Phase cycle: $\phi_1 = x,-x$; receiver $= x,-x$. (B) ^{15}N-HSQC-36N with selective F_1-scaling: The experiment yields E. COSY type multiplet patterns with J_{NN} and J_{PN} in F_1 and J_{HN} and J_{HP} in F_2, where the J_{NN} couplings are scaled $(1 + 2\chi)$-fold while the J_{PN} couplings remain unaffected. Phase cycle: $\phi_1 = 2(x,-x)$; $\phi_2 = x,x,y,y$; receiver $= x,-x,-x,x$. (C) ^{15}N-HSQC-36N with ^{15}N−^{15}N relay: The experiment generates cross peaks between ^{15}N and ^{1}H nuclei with very small J_{HN} couplings through resolved J_{HN} and J_{NN} couplings with the neighboring ^{15}N nuclei. It results in E. COSY type multiplet patterns with J_{NN} in F_1 and J_{HN} in F_2. $\tau = 1/(^2J_{NN})$. Phase cycle: $\phi_1 = 4(x,-x)$; $\phi_2 = 4(y),4(-y)$; $\phi_3 = 2(x,x,-x,-x)$; receiver $= 2(x,-x,-x,x)$.

The last ^{15}N pulse of the ^{15}N-HSQC-36N experiment (Figure 1A) has a 36° flip angle. As in small flip angle COSY,[12] this leads to E. COSY type multiplet fine structures through couplings with spins that are not effectively excited by the 36° pulse but scalar coupled to the spins precessing during t_1 and t_2. With a 36° pulse, the undesired multiplet components are suppressed to below 10% of the desired ones.[13]

Most cross peaks in the ^{15}N-HSQC-36N spectrum of **1** show two components that are well-separated in the F_1 dimension by the $^1J_{NN}$ coupling to the other ^{15}N spin within the same pyrazolyl ring. The relative displacement of the two components in the F_2 dimension corresponds to the J_{HN} coupling constant between the detected ^{1}H spin and the ^{15}N spin, which is not at the ^{15}N

(11) Sørensen, O. W.; Eich, G. W.; Levitt, M. H.; Bodenhausen, G.; Ernst, R. R. *Prog. NMR Spectrosc.* **1983**, *16*, 163−192.

(12) Aue, W. P.; Bartholdi, E.; Ernst, R. R. *J. Chem. Phys.* **1976**, *64*, 2229−2246.

(13) Griesinger, C.; Sørensen, O. W.; Ernst, R. R. *J. Chem. Phys.* **1986**, *85*, 6837−6852.

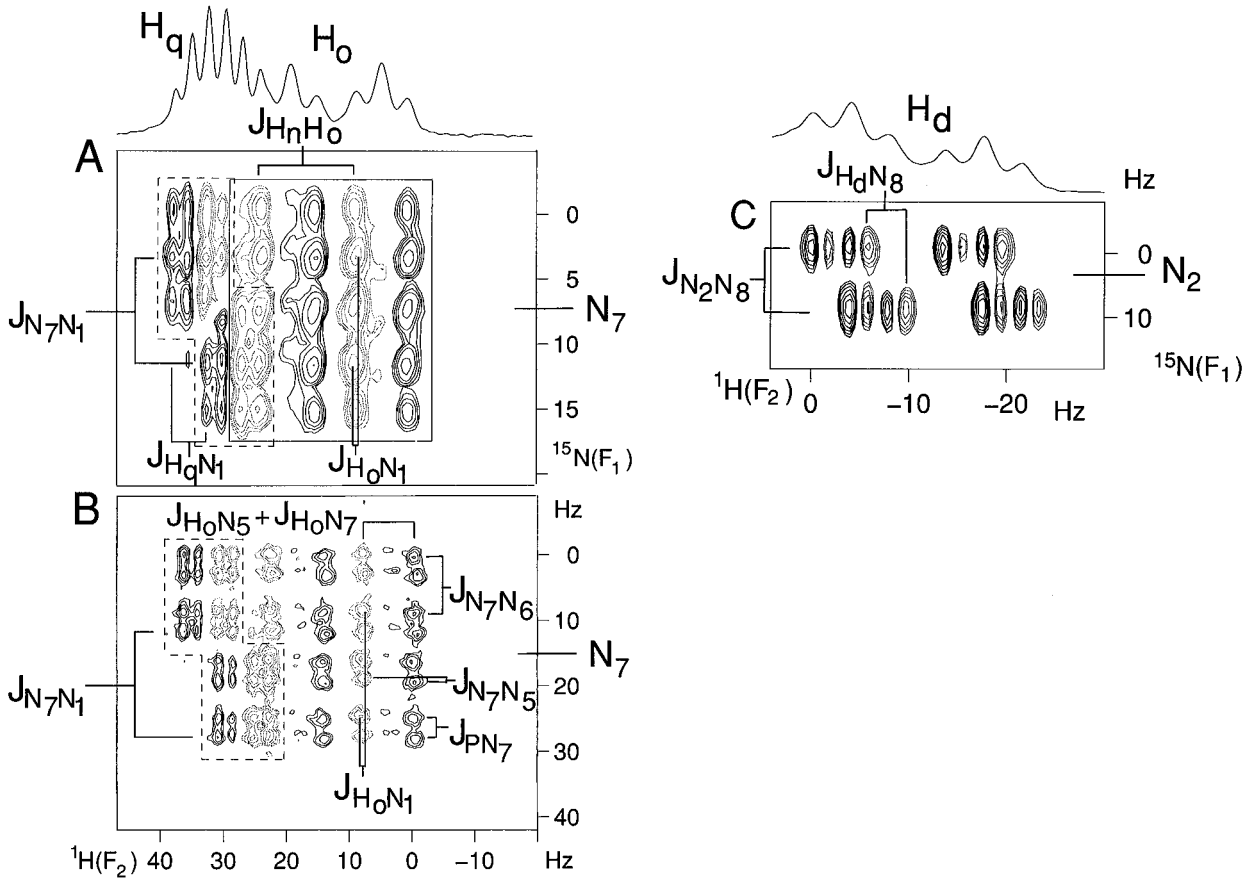

Figure 2. Selected cross peaks from the ^{15}N-HSQC-36N spectra of a 6 mM solution of **1** in CD_3OD recorded with the pulse sequences of Figure 1. Coupling constants measured from the relative displacements of the multiplet components are identified with the peaks. (A) Cross peaks N_7-H_o and N_7-H_q from the ^{15}N-HSQC-36N spectrum recorded with the experiment of Figure 1A. The overlapping cross peaks are delineated by solid and dashed lines, respectively. Experimental parameters: $\Delta = 71$ ms, $t_{1max} = 311$ ms, $t_{2max} = 1.06$ s, total experimental time 4.7 h. The selective ^{15}N pulse was a 12.5-ms hyperbolic secant pulse[35] inverting the spins N_5-N_8. (B) Same cross peaks as in part A, but from the F_1-scaled ^{15}N-HSQC-36N spectrum recorded with the pulse sequence of Figure 1B. The recording and processing parameters were identical with those of the spectrum in part A, except that $t_{1max} = 311$ ms refers to the total J-coupling evolution time ($\chi = 0.5$), and the total experimental time was 2 h. (C) Cross peak N_2-H_d recorded with the ^{15}N-HSQC-36N experiment with ^{15}N$-^{15}$N relay (Figure 1C). The coupling constant $J_{H_dN_8}$ is readily measured from the relative displacement of the cross-peak components, which are separated in F_1 by the $^1J_{N_2N_8}$ coupling constant. The negative tilt of the cross peak indicates that the sign of $J_{H_dN_8}$ is opposite to that of $^1J_{N_2N_8}$. Experimental parameters: $\Delta = 71$ ms, $\tau = 58$ ms, $t_{1max} = 155$ ms, $t_{2max} = 1.06$ s, experimental time 3 h. The selective ^{15}N pulse was a 12.5-ms hyperbolic secant pulse inverting the spins N_5-N_8.

frequency of the cross peak. The situation is more complicated for the cross peaks with N_7, which turned out to have a $^2J_{NN}$ coupling of 4.3 Hz to N_6 and a $^2J_{PN}$ coupling of 2.9 Hz to the ^{31}P spin in addition to the $^1J_{NN}$ coupling of 8.5 Hz to N_1. Figure 2A shows the partially overlapping cross peaks N_7-H_q and N_7-H_o from the ^{15}N-HSQC-36N spectrum of **1**. At the resolution of the spectrum in the F_1 dimension, the components of the doublet arising from the $^1J_{NN}$ coupling constant each appear to be split into a triplet by the $^2J_{NN}$ and $^2J_{PN}$ couplings, with overlap between the closest components of the two apparent triplets. The J_{HN} couplings can be measured from the displacement of the central components of the apparent triplets along the F_2 frequency axis as indicated in Figure 2A, but the couplings $^2J_{NN}$ and $^2J_{PN}$ cannot be measured from this cross peak.

A ^{15}N-HSQC-36N experiment with selective F_1 scaling was used to resolve the couplings $^2J_{NN}$ and $^2J_{PN}$ (Figure 1B). The pulse sequence is identical with that of the ^{15}N-HSQC-36N experiment, except that the evolution time for the J_{NN} couplings is increased $(1 + 2\chi)$-fold, while it remains unchanged for the J_{PN} couplings. In contrast to nonselective F_1-scaling,[14] selective F_1 scaling results in an altered multiplet fine structure in the F_1 dimension. Figure 2B shows the same cross peaks as in Figure 2A, but recorded with the F_1-scaled ^{15}N-HSQC-36N experiment. All eight multiplet components due to the couplings $^1J_{N_7N_1}$, $^2J_{N_7N_6}$ and $^2J_{PN_7}$ are resolved in the F_1 dimension, and their values are readily measured from the multiplet pattern. In addition, the small coupling $^2J_{N_7N_5}$ is resolved in the multiplet pattern (see below).

For J_{HN} coupling constants smaller than about 0.5 Hz, the cross peaks observed in the ^{15}N-HSQC experiments were very weak or absent. A ^{15}N-HSQC-36N experiment with ^{15}N$-^{15}$N relay (Figure 1C) was used to enhance these weak correlation peaks. In this experiment, the resolved J_{HN} coupling to a ^{15}N spin N_a, for example, is used to create the coherence H_xN_{az} by the end of the INEPT delay Δ. After the spin-lock purge pulse, this coherence is converted into H_zN_{ay} by the following 90° pulses and further into H_zN_{by} through the following ^{15}N$-^{15}$N relay step. The antiphase magnetization H_yN_{bz} is detected during the acquisition time. The ^{15}N$-^{15}$N relay step intermittently generates the term $H_zN_{az}N_{bx}$ after the fourth ^{15}N pulse of the pulse sequence. The following delay (Figure 1C) serves to refocus the ^{15}N$-^{15}$N coupling. In principle, the experiment could also be recorded without this refocusing delay, using the evolution time t_1 for refocusing. The only inconvenience would be that the FID recorded with $t_1 = 0$ would contain no signal, since the resulting cross peaks would be antiphase with respect to the ^{15}N$-^{15}$N coupling. The observation of the cross peaks in the ^{15}N-HSQC-36N experiment with ^{15}N$-^{15}$N relay depends on the presence of a finite coupling between spins H and N_b,

(14) Brown, L. R. *J. Magn. Reson.* **1984**, *57*, 513−518.

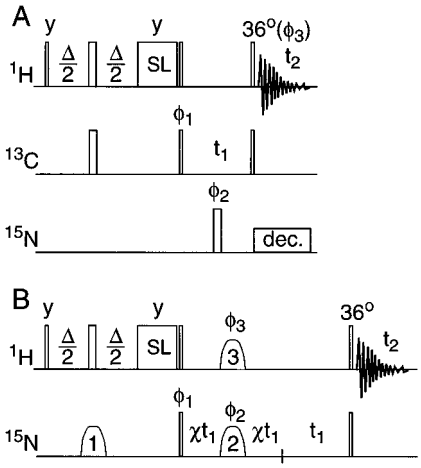

Figure 3. Pulse sequences relating the sign of J_{HN} to that of $^1J_{HC}$. In both experiments, the last ^{1}H pulse is a 36° pulse. (A) ^{13}C-HSQC-36H: The experiment relates the sign of $^3J_{HH}$ to that of $^1J_{HC}$ through an E.COSY type multiplet pattern with $^1J_{HC}$ in F_1 and $^3J_{HH}$ in the F_2 dimension. $\Delta = 1/(2\,^2J_{HC})$. Phase cycle: $\phi_1 = 4(x,-x)$; $\phi_2 = 2(x,x,-x,-x)$; $\phi_3 = 4(x),4(-x)$; receiver $= 2(x,-x),2(-x,x)$. (B) ^{15}N-HSQC-36H with F_1 scaling. The experiment relates the sign of J_{HN} to that of $^3J_{HH}$ through E.COSY type multiplet patterns with J_{HN} in F_1 and $^3J_{HH}$ in F_2. $\Delta = 1/(^2J_{HN})$. Selective pulses: 1, 180°(^{15}N) inversion pulse inverting a subset of the ^{15}N resonances; 2, 180°(^{15}N) refocusing pulse acting on the same subset of ^{15}N spins; 3, 180°(^{1}H) inversion pulse acting on the protons for which the J_{HN} couplings with the ^{15}N spins refocused by the selective pulse 2 are to be scaled in the F_1 dimension. Phase cycle: $\phi_1 = 4(x,-x)$; $\phi_2 = 2(x,x,y,y)$; $\phi_3 = 4(x),4(-x)$; receiver $= 2(x,-x,-x,x)$.

but their intensities are much improved over the experiment without ^{15}N−^{15}N relay, since the experiment does not rely on the evolution of small J_{HN} couplings during the delay Δ. To measure J_{HN} couplings with high accuracy, long acquisition times t_{2max} have to be chosen anyway. During a long acquisition time, antiphase magnetization can refocus into observable in-phase magnetization also through small J_{HN} couplings.

Determination of the Absolute Signs of the Homo- and Heteronuclear Coupling Constants. The absolute signs of the scalar coupling constants can be determined by relating their signs to the sign of a positive one-bond ^{1}H−^{13}C coupling.[15] The ^{13}C-HSQC-36H experiment (Figure 3A) was used to relate the sign of the $^3J_{H_bH_c}$ coupling to the sign of the $^1J_{H_bC_b}$ coupling. The experiment also relates the signs of the corresponding $^3J_{HH}$ and $^1J_{HC}$ couplings in the other pyrazolyl spin systems to each other (Figure 4A). As in a regular ^{13}C-HSQC experiment, homonuclear ^{1}H−^{1}H couplings do not contribute to the multiplet fine-structure in the F_1 dimension. J_{CN} and J_{HN} couplings are effectively decoupled by respectively the 180°(^{15}N) pulse during t_1 and ^{15}N broadband decoupling during t_2. The positive tilt of the cross peaks shows that the $^3J_{HH}$ couplings have the same sign as the $^1J_{HC}$ couplings.

The signs of the J_{HN} couplings can be related to the signs of the $^3J_{HH}$ couplings by an analogous experiment performed with ^{15}N instead of ^{13}C in the indirectly detected frequency dimension. Since the J_{HN} couplings are smaller than or of comparable size to the $^1J_{NN}$ couplings, an F_1-scaled version of the ^{15}N-HSQC-36H experiment was designed to selectively scale the J_{HN} couplings without scaling the J_{NN} couplings. The pulse sequence is shown in Figure 3B. The selective scaling of the J_{HN} couplings is achieved by the element χt_1−180°(^{1}H,^{15}N)−χt_1, where the 180°(^{15}N) pulse is a selective refocusing pulse and the 180°(^{1}H) pulse a selective inversion pulse. The spectrum of Figure 4B was recorded with a RE-BURP pulse[16] selectively refocusing the ^{15}N resonances of N_1 to N_4, and a G^3 pulse[17] selectively inverting the ^{1}H resonances H_b, H_g, H_q, and H_l. With $\chi = 1.5$, a J_{HN} coupling of 5 Hz appears as a 20-Hz coupling, which is significantly larger than the $^1J_{NN}$ couplings that are of the order of 8 to 9 Hz. It is then sufficient to record the experiment with only moderate digital resolution in the F_1 dimension to observe the E.COSY type tilt of the cross peaks. The positive tilt observed for the cross peaks in Figure 2 indicates that the sign of the J_{HN} couplings is positive like the sign of the $^3J_{HH}$ couplings. Since the N−H cross peaks with the protons H_c, H_f, H_p, and H_m show negative tilts in the ^{15}N-HSQC-36N experiment, the $^1J_{NN}$ couplings are negative, in accordance with literature.[18,8] This experiment also determines the sign of all other J_{HN} couplings that have not directly been related to the sign of a $^3J_{HH}$ coupling, since they were correlated to the sign of the $^1J_{NN}$ couplings by the ^{15}N-HSQC-36N experiments.

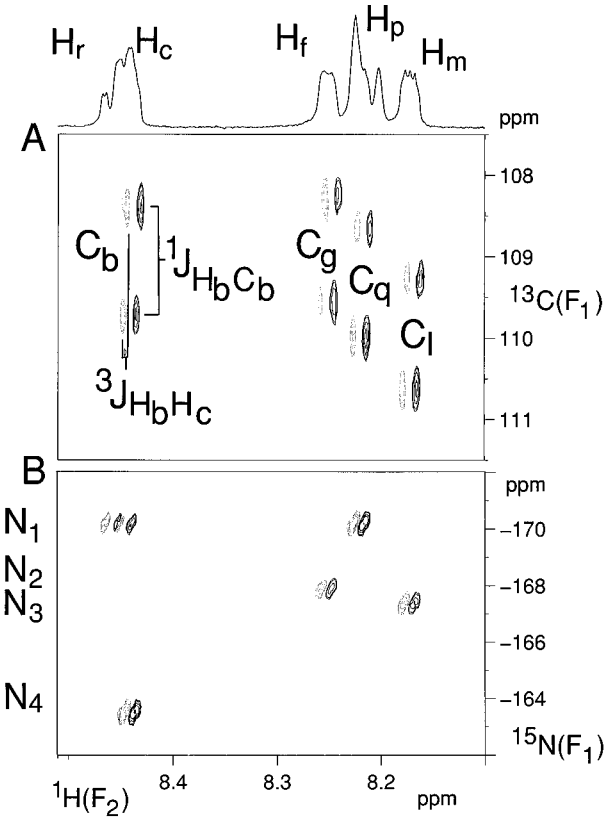

Figure 4. Selected spectral regions from ^{13}C-HSQC-36H and ^{15}N-HSQC-36H spectra recorded with the pulse sequences of Figure 3 and the sample of Figure 2. (A) ^{13}C-HSQC-36H cross peaks between C_b−H_c, C_g−H_f, C_q−H_p, and C_l−H_m, respectively. The positive tilt of the cross peaks shows that the couplings $^3J_{H_bH_c}$, $^3J_{H_gH_f}$, $^3J_{H_qH_p}$, and $^3J_{H_lH_m}$ have the same sign as $^1J_{H_bC_b}$, $^1J_{H_gC_g}$, $^1J_{H_qC_q}$, and $^1J_{H_lC_l}$, respectively. Experimental parameters: $\Delta = 100$ ms, $t_{1max} = 256$ ms, $t_{2max} = 530$ ms, total experimental time 4 h. (B) Cross peaks N_1−H_p, N_2−H_f, N_3−H_m, and N_4−H_c from a ^{15}N-HSQC-36H spectrum with F_1 scaling. In addition, the cross peak N_1−H_r is observed. The positive tilt of the cross peaks shows that the couplings $J_{H_qN_1}$, $J_{H_gN_2}$, $J_{H_lN_3}$, and $J_{H_bN_4}$ have the same sign as $^3J_{H_qH_p}$, $^3J_{H_gH_f}$, $^3J_{H_lH_m}$, and $^3J_{H_bH_c}$. Experimental parameters: $\Delta = 71$ ms, $t_{1max} = 311$ ms (including the J-evolution period $2\chi t_1$ with $\chi = 1.5$), $t_{2max} = 1.06$ s, total experimental time 45 min. Selective pulses used: 1, hyperbolic secant of 12.5-ms duration selectively inverting nitrogens 1−4; 2, RE-BURP pulse[16] of 10-ms duration selectively refocusing nitrogens 1−4; 3, G^3 pulse[17] of 23-ms duration selectively inverting the spins H_b, H_g, H_q, and H_l.

(15) Kowalewski, J. *Prog. NMR Spectrosc.* **1977**, *11*, 1−78.
(16) Geen, H.; Freeman, R. J. Magn. Reson. **1991**, *93*, 93−141.
(17) Emsley, L.; Bodenhausen, G. *Chem. Phys. Lett.* **1990**, *165*, 469−476.
(18) Berkhoudt, T.; Jakobsen, H. J. *J. Magn. Reson.* **1982**, *50*, 323−327. Kuroda, Y.; Fujiwara, Y.; Matsushita, K. *J. Chem. Soc., Perkin Trans. 2* **1985**, 1533−1536.

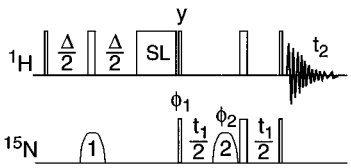

Figure 5. Pulse sequence of an F_1-decoupled ^{15}N-HSQC experiment. The pulse sequence generates an E. COSY type multiplet pattern from which J_{HP}, J_{PN}, and their relative signs can be measured. $\Delta = 1/(^2J_{HN})$. Selective ^{15}N pulses: 1, 180° pulse inverting either the metal ligating or the remote ^{15}N spins; 2, 180° refocusing pulse selective for a single one of the group of ^{15}N spins excited by the selective pulse 1. The selective ^{15}N refocusing pulse provides effective homonuclear J_{NN} decoupling during t_1. Phase cycle: $\phi_1 = 2(x,-x)$; $\phi_2 = 2(x),2(y)$; receiver $= x,-x,-x,x$.

Determination of ^{1}H−^{31}P and ^{31}P−^{15}N Coupling Constants. Besides splittings due to J_{NN}, the cross peaks in the ^{15}N-HSQC experiments are split by passive couplings with respect to ^{31}P yielding J_{PN} and J_{HP} in the F_1 and F_2 dimensions, respectively. The J_{PN} and J_{HP} coupling constants are most easily measured from a F_1-decoupled ^{15}N-HSQC experiment (Figure 5). F_1 decoupling is achieved by the combination of a selective 180°(^{15}N) refocusing pulse together with a nonselective 180°-(^{15}N) pulse in the middle of the evolution time t_1. Similar to F_1-decoupled NOESY experiments,[19] the homonuclear couplings between the selectively refocused nitrogen and the other nitrogens are effectively decoupled in the F_1 frequency dimension. Selective refocusing of a single ^{15}N resonance retains the J_{PN} couplings as the only couplings in the F_1 dimension. Since ^{31}P is not pulsed during the experiment, an E. COSY type multiplet pattern results from which the coupling constants J_{PN} and J_{HP} can be read in the F_1 and F_2 dimension, respectively.

Eight different F_1-decoupled ^{15}N-HSQC experiments were recorded with the selective 180°(^{15}N) refocusing pulse applied to each of the eight individual ^{15}N resonances of **1**. The 180°-(^{15}N) inversion pulse (1, Figure 5) was selectively applied to all of the resonances N_1 to N_4 to achieve efficient magnetization transfer during the INEPT step, while the 180°(^{15}N) refocusing pulse (2, Figure 5) selected each of these four ^{15}N spins in turn. In addition, the 180°(^{15}N) inversion pulse (1, Figure 5) was selectively applied to all of the resonances N_5 to N_8, while the 180°(^{15}N) refocusing pulse (2, Figure 5) selected each of the four ^{15}N spins N_5, N_6, N_7, and N_8 in turn. J_{PN} couplings could be resolved for the ^{15}N signals of N_2, N_5, N_6, N_7, and N_8 (*e.g.* Figure 6A). No J_{PN} splitting could be resolved for the other ^{15}N resonances which, at the resolution of the experiments, places an upper limit of |0.4| Hz to their couplings with the phosphorus.

The J_{HP} couplings were also determined from the F_1-decoupled ^{15}N-HSQC experiment (Figure 5) and confirmed by the analysis of the multiplet fine structure of the ^{15}N−^{1}H cross peaks in the undecoupled ^{15}N-HSQC-36N experiments (e.g. Figure 2B). These experiments also determine the relative sign of the J_{HP} and J_{PN} couplings. The absolute sign of the $^2J_{PN_8}$ coupling was determined by a simple ^{31}P-HSQC experiment recorded with an INEPT delay of 100 ms. No pulses were applied at the ^{15}N frequency, resulting in E. COSY type multiplets with respect to the large $^2J_{PN_8}$ coupling in F_1 and the respective J_{HN_8} coupling in the F_2 dimension. Figure 6B shows the cross peak P−H_f from the ^{31}P-HSQC spectrum. The $^2J_{PN_8}$ coupling constant is 43.3 Hz and easily resolved in the F_1 dimension. The poorly resolved, positive tilt of the cross peak shows that the sign of the J_{PN_8} coupling is the same as that of the $J_{H_fN_8}$ coupling, which had been determined as positive (see above). Other J_{PN} couplings are much smaller and difficult to resolve in this experiment, because of the relatively rapid ^{31}P relaxation. The positive tilt observed in the cross peak of Figure 6B within each of the multiplet components of the doublet made by the J_{PN_8} coupling originates from the couplings J_{PN_2} and $J_{H_fN_2}$, which were more accurately determined from the ^{15}N-HSQC experiments. The ^{31}P-HSQC experiment yielded cross peaks with H_f, H_g, H_h, H_n, and H_o, identifying these as the protons with the largest coupling constants to the ^{31}P spin.

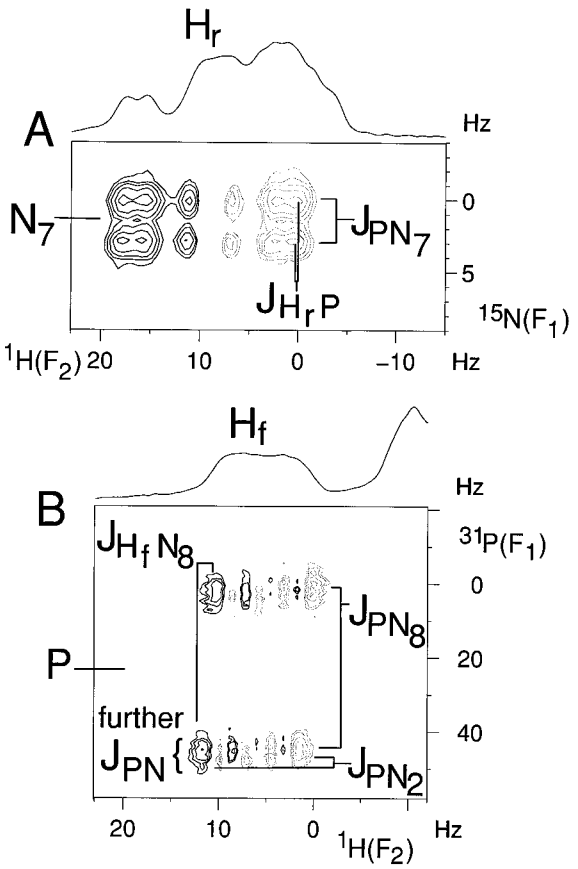

Figure 6. Selected cross peaks from the F_1-decoupled ^{15}N-HSQC experiment and from a ^{31}P-HSQC spectrum. Same sample as in Figure 2. (A) Cross peak N_7−H_r from the F_1-decoupled ^{15}N-HSQC experiment recorded with the sequence of Figure 5. The couplings J_{PN_7} and J_{H_rP} are read from the displacements of the multiplet components in the F_1 and F_2 dimension, respectively. The positive tilt of the cross peak shows that J_{PN_7} and J_{H_rP} have the same sign. Experimental parameters: $\Delta =$ 71 ms, $t_{1max} = 768$ ms, $t_{2max} = 1.06$ ms, experimental time 30 min. Selective ^{15}N pulses: 1, 12.5 ms hyperbolic secant pulse[35] inverting N_5−N_8; 2, 70 ms RE- BURP pulse[16] acting on N_7. (B) Cross peak between the ^{31}P resonance and H_f in the ^{31}P-HSQC spectrum. Experimental parameters: total duration of the INEPT delay: 100 ms, $t_{1max} = 426$ ms, $t_{2max} = 1.06$ s, total experimental time about 16 h.

Determination of Small ^{15}N−^{15}N Coupling Constants. The ^{15}N-HSQC-36N experiment with selective F_1 scaling clearly reveals two further J_{NN} couplings besides the $^1J_{NN}$ coupling (Figure 2B). The assignment of these J_{NN} couplings was achieved by a quantitative long-range ^{15}N−^{15}N (LRNN) correlation experiment. As in the original experiments developed for *J*-coupling measurements in isotope enriched proteins,[20] the LRNN correlation experiment is an "out-and-back" experiment, where the magnitudes of the J_{NN} coupling constants are encoded in the cross-peak intensities. Figure 7A shows the pulse sequence of the quantitative LRNN correlation experiment. First,

(19) Brüschweiler, R.; Griesinger, C.; Sørensen, O. W.; Ernst, R. R. *J. Magn. Reson.* **1988**, *78*, 178−185. Otting, G.; Orbons, L. P. M.; Wüthrich, K. *J. Magn. Reson.* **1990**, *89*, 423−430.

(20) Bax, A.; Max, D.; Zax, D. *J. Am. Chem. Soc.* **1992**, *113*, 6924−6925. Vuister, G. W.; Yamazaki, T.; Torchia, D. A.; Bax, A. *J. Biomol. NMR* **1993**, *3*, 297−306. Vuister, G. W.; Bax, A. *J. Magn. Reson. B* **1993**, *102*, 228−231.

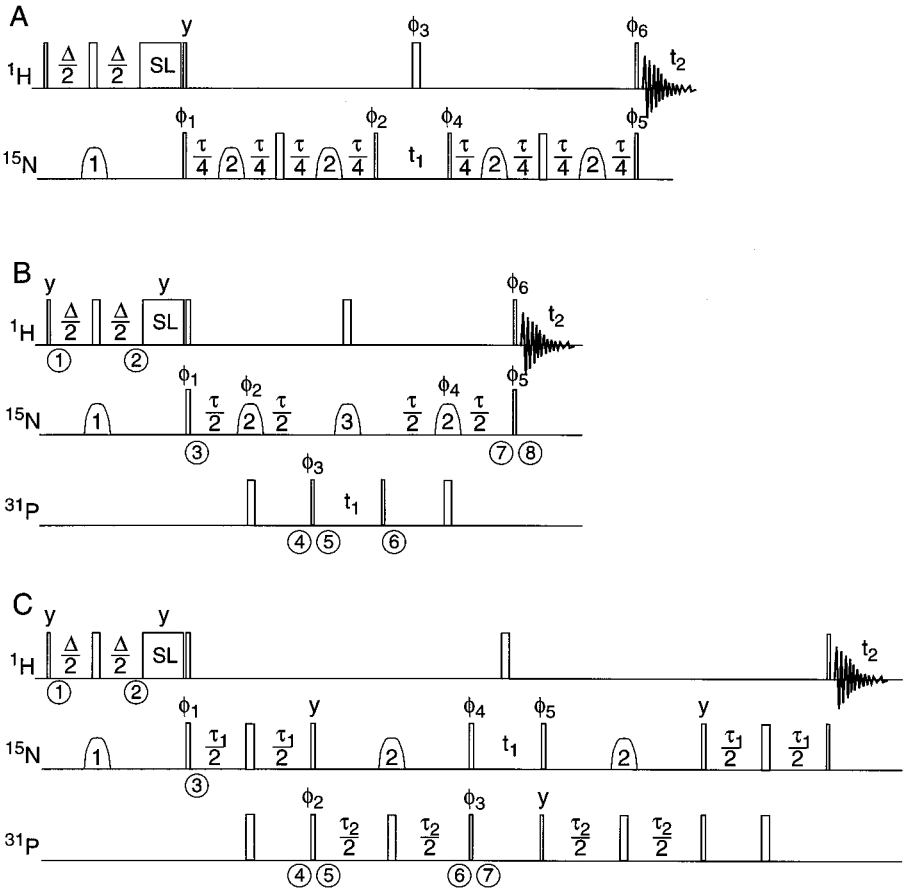

Figure 7. Pulse sequences for the measurement of size and sign of J_{NN} couplings, and the sign of J_{PN} couplings. (A) Quantitative long-range $^{15}N-^{15}N$ (LRNN) correlation experiment. The experiment is an "out-and-back" experiment with the magnetization transfer $H_y \rightarrow H_zN_{ay} \rightarrow H_zN_{az}N_{bx}$ and back. The coupling constant J_{NN} is measured from the relative peak intensities of the N_a-H and N_b-H cross peaks: $I(N_b-H)/I(N_a-H) = \sin^2(\pi J\tau)/\cos^2(\pi J\tau)$. All selective ^{15}N pulses are 180° inversion pulses. The selective pulse 1 acts on the four low-field ^{15}N resonances, if the selective pulse 2 acts on the four high-field ^{15}N resonances, or vice versa. The selectivity of these pulses helps to direct the ^1H magnetization to the nitrogens of interest in the INEPT step and to refocus the $^1J_{NN}$ couplings during the relay periods. $\Delta = 1/(^2J_{HN})$, $\tau = 1/(^2J_{NN})$. Phase cycle: $\phi_1 = 32(x,-x)$; $\phi_2 = 16(y,y,-y,-y)$; $\phi_3 = 32(x),32(-x)$; $\phi_4 = 8[4(y),4(-y)]$; $\phi_5 = 4[8(x),8(-x)]$; $\phi_6 = 2[16(x),16(-x)]$; receiver = $2[4(x,-x),8(-x,x),4(x,-x)]$. (B) DQ/ZQ-PN experiment. The experiment generates mixed DQ/ZQ coherence between ^{15}N and ^{31}P via the magnetization transfer pathway $H_x \rightarrow H_zN_y \rightarrow H_zN_xP_y$. The selective ^{15}N pulses are the following: 1, 180° inversion pulse acting on the metal coordinating ^{15}N spins; 2, 180° refocusing pulse acting on a single one of the ^{15}N spins excited by the selective pulse 1; 3, 180° inversion pulse for the group of four ^{15}N spins remote from the metal coordination sphere. $\Delta = 1/(^2J_{HN})$, $\tau = 1/(^2J_{PN})$. Phase cycle: $\phi_1 = 32(x,-x)$; $\phi_2 = 16(x,x,y,y)$; $\phi_3 = 8[4(x),4(-x)]$; $\phi_4 = 4[8(x),8(y)]$; $\phi_5 = 2[16(x),16(-x)]$; $\phi_6 = 32(x),32(-x)$; receiver = $x,-x,-x,x,2(-x,x,x,-x),x,-x,-x,x,2[-x,x,x,-x,2(x,-x,-x,x),-x,x,x,-x],x,-x,-x,x,2(-x,x,x,-x),x,-x,-x,x$. Numbers in circles indicate the time points for which the product operator terms are discussed in the text. (C) DQ/ZQ-NN experiment. The experiment generates mixed DQ/ZQ coherence between two ^{15}N spins via the magnetization transfer pathway $H_x \rightarrow H_zN_{ay} \rightarrow H_zN_{az}P_y \rightarrow H_zN_{az}P_yN_{bz} \rightarrow H_zN_{ay}P_zN_{by}$. The selective ^{15}N pulses are the following: 1, 180° inversion pulse acting on the metal coordinating ^{15}N spins; 2, 180° inversion pulse acting on a single one of the excited ^{15}N spins (N_b). $\Delta = 1/(^2J_{HNa})$, $\tau_1 = 1/(^2J_{PNa})$, $\tau_2 = 1/(^2J_{PNb})$. Phase cycle: $\phi_1 = 16(x,-x)$; $\phi_2 = 4[4(x),4(-x)]$; $\phi_3 = 2[8(y),8(-y)]$; $\phi_4 = 8(x,x,-x,-x)$; $\phi_5 = 16(x),16(-x)$; receiver = $2[x,-x,x,-x,2(-x,x,-x,x),x,-x,x,-x]$.

antiphase coherence is created with respect to one of the ^{15}N spins coordinating the metal ion. This coherence is relayed through J_{NN} couplings to any of the other ^{15}N spins, frequency labeled during t_1, and relayed back through the same pathway. Denoting the proton and nitrogen spins as H, N_a, and N_b, respectively, the relevant product operator terms immediately preceeding the 90°(^{15}N) pulse before t_1 are H_zN_{ay} and $H_zN_{ax}N_{bz}$. The 90°(^{15}N) pulse converts these terms into H_zN_{ay} and $H_zN_{az}N_{bx}$, which subsequently precess during t_1 with the frequencies of N_a and N_b, respectively. The cross peaks $N_a \rightarrow H$ and $N_b \rightarrow H$ identify the nitrogen spins connected through J_{NN}. Their intensities depend on the relay delays preceeding and following the evolution time t_1 with $\cos^2(\pi J\tau)$ and $\sin^2(\pi J\tau)$, respectively. Assuming identical relaxation of both terms, the coupling constant can readily be calculated from the relative volume of the two cross peaks.[20]

Figure 8A shows a few spectral regions of the LRNN correlation experiment. The most intense cross peaks are the "parent peaks" that also occur in regular ^{15}N-HSQC spectra. The weaker cross peaks are the relayed peaks that occur only in the LRNN correlation experiment. Parent and relayed peaks are of opposite sign, because the relayed peak originates from magnetization that is defocused and refocused by the J_{NN} coupling according to $N_{ax} \rightarrow N_{ay}N_{bz} \rightarrow -N_{ax}$, while the magnetization of the parent peak represents that part of the magnetization that did not evolve with the J_{NN} coupling. The relayed peaks in Figure 8A clearly demonstrate J_{NN} couplings between N_6 and N_7, N_5 and N_7, and N_6 and N_8, but not between N_5 and N_6 or N_7 and N_8. The spectrum of Figure 8A was recorded with a $^{15}N-^{15}N$ relay delay of 250 ms for which a J_{NN} coupling of 2 Hz would lead to complete magnetization transfer. Evaluating the relative intensities of relayed and parent peaks, we determined $|J_{N_6N_7}| = 4.3$ Hz, $|J_{N_5N_7}| = 0.3$ Hz, and $|J_{N_6N_8}| = 0.2$ Hz, while $|J_{N_5N_6}|$ and $|J_{N_7N_8}|$ must be smaller than 0.2 Hz. The sign of the cis couplings $J_{N_5N_7}$ and $J_{N_6N_8}$ is negative, as revealed by the negative tilt of the multiplet fine structures of the N_7-H_o and N_6-H_d cross peaks in the ^{15}N-HSQC-36N spectrum with F_1 scaling (Figure 2B). The sign of the trans coupling $J_{N_6N_7}$ could not be determined from the ^{15}N-HSQC-36N spectra, since none of the proton spins has resolved

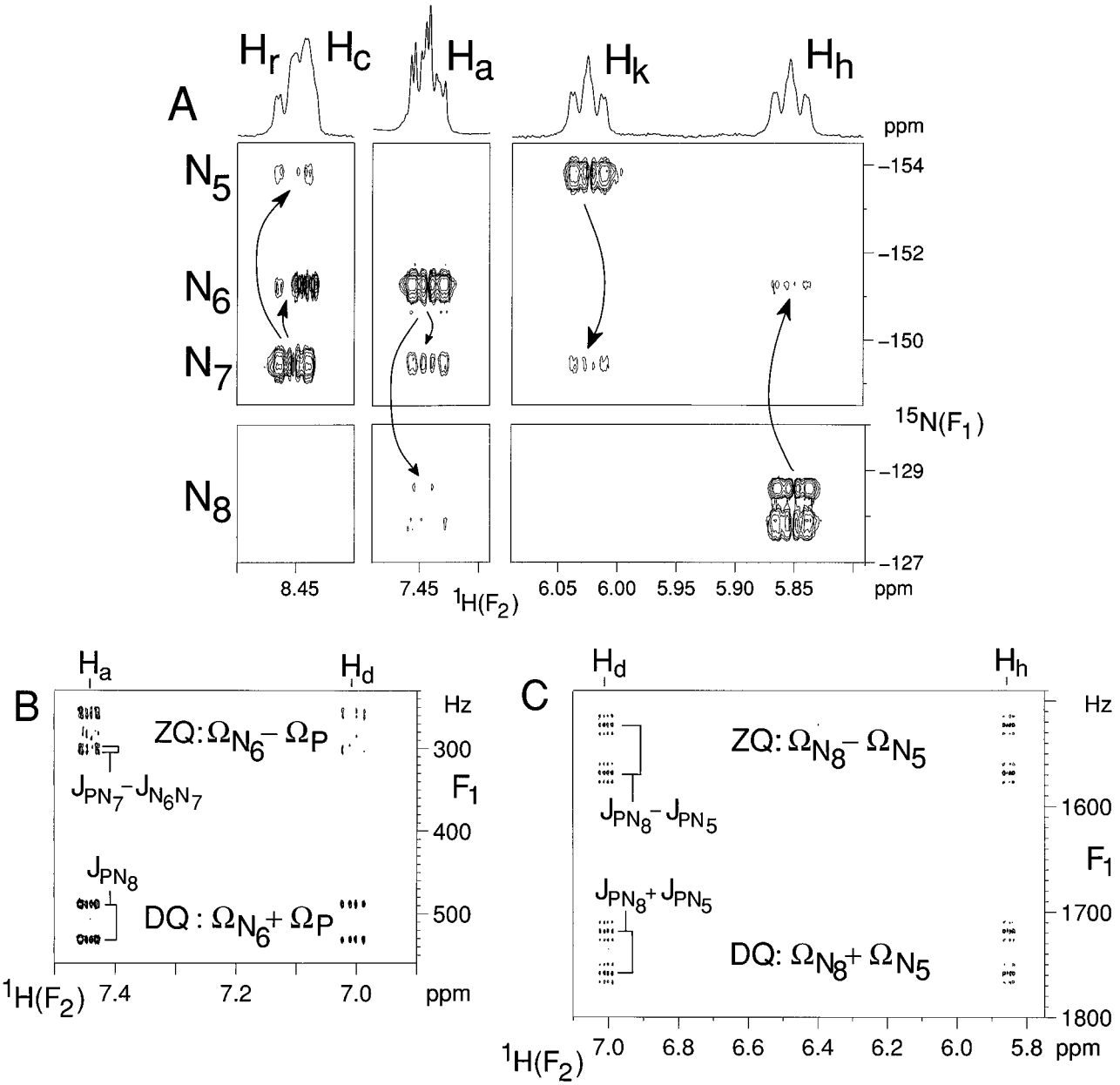

Figure 8. Selected spectral regions from the quantitative long-range $^{15}N-^{15}N$ (LRNN) correlation experiment, the DQ/ZQ-PN experiment and the DQ/ZQ-NN experiment recorded with the pulse sequences of Figure 7. Same sample as in Figure 2. (A) LRNN correlation spectrum. The resonance assignments are indicated. The most intense peaks (N_5-H_k, N_6-H_c, N_6-H_a, N_7-H_r, and N_8-H_h) are direct correlations. The relayed cross peaks between them indicate small $^2J_{NN}$ couplings across the metal center. Arrows point from the direct correlation peaks to the relayed cross peaks. Experimental parameters: $\Delta = 58$ ms, $\tau = 250$ ms, $t_{1max} = 30$ ms, $t_{2max} = 1.06$ s, total experimental time 6 h. (B) DQ and ZQ cross peaks from the DQ/ZQ-PN experiment. The DQ and ZQ frequencies and the splitting due to J_{NN} and J_{PN} couplings are identified. Experimental parameters: $\Delta = 71$ ms, $\tau = 170$ ms, $t_{1max} = 240$ ms, $t_{2max} = 1.06$ s, total experimental time about 11.5 h. Selective ^{15}N pulses: 1, 12.5 ms hyperbolic secant pulse[35] applied to N_5 to N_7; 2, 60 ms RE-BURP pulse[16] applied to N_6; 3, 12.5 ms hyperbolic secant pulse applied to N_1 to N_4. The first 21 points in the t_1 dimension were generated by linear prediction to account for the delayed acquisition caused by the selective ^{15}N inversion pulse in the middle of t_1. (C) DQ and ZQ cross peaks from the DQ/ZQ-NN experiment. The multiplet splittings due to J_{PN} couplings in the F_1 dimension are identified. Experimental parameters: $\Delta = 71$ ms, $\tau_1 = 11$ ms, $\tau_2 = 100$ ms, $t_{1max} = 266$ ms, $t_{2max} = 1.06$ s, total experimental time about 14.3 h. Selective ^{15}N pulses: 1, 12.5 ms hyperbolic secant pulse centered at the frequency of N_8; 2, 35 ms G^3 pulse[17] applied to N_5. The F_1 frequency axes in (B) and (C) are labeled with respect to the carrier frequency.

couplings to both nitrogens simultaneously. This sign was determined from a DQ/ZQ experiment (see below).

The spectrum of Figure 8A was recorded with semiselective ^{15}N inversion pulses applied to N_1 to N_4 during the relay delays to avoid the generation of relayed peaks via the $^1J_{NN}$ couplings. To check for $^3J_{NN}$ couplings across the metal center, a quantitative LRNN correlation experiment was also recorded without these selective 180°(^{15}N) inversion pulses to enable the evolution of antiphase coherence of the ^{15}N spins of N_5, N_6, N_7, and N_8 with respect to the spins of N_1, N_2, N_3, and N_4. The trivial transfer of coherence through the large $^1J_{NN}$ couplings was minimized by choosing a relay delay of 118 ms $\approx 1/^1J_{NN}$. No cross peaks were observed between remote nitrogen spins in this experiment, placing an upper limit of 0.3 Hz on the magnitude of any of the $^3J_{NN}$ couplings across the metal center. The absence of sizable $^3J_{NN}$ couplings is independently confirmed by the absence of further multiplicity in the ^{15}N NMR signals (e.g. Figure 2B).

The double quantum/zero quantum (DQ/ZQ) experiment[21] relates the sign of the coupling J_{AM} to the sign of the coupling J_{MX} in a linear 3-spin system A−M−X, when $J_{AX} = 0$.[22] Using

(21) Rexroth, A.; Schmidt, P.; Szalma, S.; Geppert, T.; Schwalbe, H.; Griesinger, C. *J. Am. Chem. Soc.* **1995**, *117*, 10389−10390. Jarvet, J.; Allard, P. J. *J. Magn. Reson. B* **1996**, *112*, 240−244.

the DQ/ZQ-PN experiment of Figure 7B, the unknown sign of $J_{N_6N_7}$ was related to the sign of the coupling $^2J_{PN_7}$, which in turn was related to the known sign of the coupling $^2J_{PN_8}$ by the DQ/ZQ-NN experiment of Figure 7C.

The pulse sequence of Figure 7B generates the coherence $H_{az}N_{6x}P_y$ through the magnetization transfer pathway at the time points indicated in the Figure: $H_{ax}(1) \rightarrow H_{ay}N_{6z}(2) \rightarrow H_{az}N_{6y}(3) \rightarrow H_{az}N_{6x}P_z(4) \rightarrow H_{az}N_{6x}P_y(5)$. This magnetization transfer was optimized by the use of selective 180°(^{15}N) pulses (labeled 1 and 2 in Figure 7B) that were applied to N_5-N_7 and N_6, respectively. The coherence $H_{az}N_{6x}P_y$ is mixed DQ and ZQ coherence, which evolves during the evolution time t_1 with the sum and the difference of the ^{15}N and ^{31}P frequencies Ω_{N_6} and Ω_P with respect to the ^{15}N and ^{31}P carrier frequencies. The coherence $H_{az}N_{6x}P_y$ present at the end of the evolution time t_1 is refocused via $H_{az}N_{6x}P_z(6)$ and $H_{az}N_{6y}(7)$, and the antiphase magnetization $H_{ay}N_{6z}(8)$ is detected during the acquisition time. The DQ and ZQ components of the coherence $H_{az}N_{6x}P_y$ evolve with the sum and the difference of the couplings of N_6 and P with the common coupling partner N_7. Couplings with N_1-N_4 were refocused by a selective 180°(^{15}N) inversion pulse applied to N_1-N_4 (labeled 3 in Figure 7B).

The identification of the DQ and ZQ peaks is not complicated by the absolute signs of the magnetogyric ratios of the ^{15}N and ^{31}P spins, since current NMR spectrometers operate with linear as opposed to circular radio frequency fields, measuring the absolute value of the precession frequencies relative to the carrier frequency without distinction between positive and negative Larmor frequencies. Placing the respective carriers at the high-field ends of the ^{15}N and ^{31}P resonances consistently results in larger frequencies for the DQ coherence than for the ZQ coherence.

Figure 8B shows the spectrum recorded with the DQ/ZQ-PN experiment of Figure 7B. Cross peaks are observed at the F_2 frequencies of H_a and H_d, which are the protons with the largest coupling constants with N_6 (9.7 and 4.2 Hz). The multiplet fine structure of the cross peaks in the F_1 dimension is dominated by the large $^2J_{PN_8}$ coupling. In addition, the splitting due to $^2J_{PN_7} - J_{N_6N_7}$ is observed for the zero-quantum cross peaks at $\Omega_{N_6} - \Omega_P$, while the splitting $^2J_{PN_7} + J_{N_6N_7}$ is not resolved for the double-quantum cross peaks at $\Omega_{N_6} + \Omega_P$. This shows that $^2J_{PN_7}$ and $J_{N_6N_7}$ are of opposite sign.

The magnitudes of the cis-$^2J_{PN}$ couplings range between 2.7 and 2.9 Hz. Their absolute sign was determined by the DQ/ZQ-NN experiment of Figure 7C. It generates the coherence $H_{dz}N_{8y}P_zN_{5y}$ by the pathway $H_{dx}(1) \rightarrow H_{dy}N_{8z}(2) \rightarrow H_{dz}N_{8y}(3) \rightarrow H_{dz}N_{8x}P_z(4) \rightarrow H_{dz}N_{8z}P_y(5) \rightarrow H_{dz}N_{8z}P_xN_{5z}(6) \rightarrow H_{dz}N_{8y}P_zN_{5y}(7)$. This magnetization transfer was optimized by the use of selective 180°(^{15}N) pulses (labeled 1 and 2 in Figure 7C), which were applied to N_8 and N_5, respectively. The experiment yields at the same time the corresponding coherence with H_h instead of H_d. $H_{dz}N_{8y}P_zN_{5y}$ represents mixed DQ/ZQ coherence between spins N_5 and N_8, which evolves during the evolution time t_1 under J_{PN} and J_{NN} couplings. The phosphorus spin is a common coupling partner for both N_5 and N_8, and the sign of $^2J_{PN_8}$ is known from the ^{31}P-HSQC experiment. The spectrum of Figure 8C shows that the sum of the couplings $^2J_{PN_8}$ and $^2J_{PN_5}$ leads to a smaller splitting in the DQ cross peaks than the difference of the couplings observed in the ZQ cross peaks. Consequently, $^2J_{PN_8}$ and $^2J_{PN_5}$ are of opposite sign. Besides the multiplet splittings due to J_{PN}, splittings by the large $^1J_{NN}$ couplings of N_5 and N_8 are also resolved in the DQ and ZQ cross peaks of Figure 8C.

Placing the second selective 180°(^{15}N) pulse (labeled 2 in Figure 7C) at the frequencies of N_6 or N_7 yields experiments that relate the signs of $^2J_{PN_6}$ or $^2J_{PN_7}$, respectively, to the sign of $^2J_{PN_8}$. In this way it was confirmed that the sign of $^2J_{PN_7}$, too, was opposite to the sign of $^2J_{PN_8}$.

The DQ/ZQ experiments complete the chain of experiments to determine the absolute sign of the trans-$^2J_{NN}$ coupling across the metal center. $^2J_{N_6N_7}$ is positive, since it was determined to be of opposite sign from $^2J_{PN_7}$ by the DQ/ZQ-PN experiment. $^2J_{PN_7}$ (like all other cis-$^2J_{PN}$ couplings in **1**) is negative because its sign is opposite to that of $^2J_{PN_8}$ as determined by the DQ/ZQ-NN experiment. $^2J_{PN_8}$ is positive because the ^{31}P-HSQC experiment shows that it has the same sign as $J_{H_fN_8}$ (Figure 6B). $J_{H_fN_8}$ is positive because it has the same sign as $^3J_{H_fH_g}$, which has the same sign as $^1J_{H_gC_g}$ by the ^{15}N-HSQC-36H and ^{13}C-HSQC-36H experiments of Figure 4.

Discussion

Figure 9 summarizes the scalar coupling constants measured for **1**. The signs and sizes of all two-bond coupling constants between the metal ligating ^{15}N and ^{31}P spins were determined, except for the vanishingly small cis-$^2J_{NN}$ couplings between nitrogens of the two different bis-pyrazolyl ligands. **1** is the first example where $^2J_{NN}$ coupling constants across a metal center with octahedral coordination have been measured. As with similar couplings between ^{1}H, ^{13}C, and ^{31}P spins, the trans-$^2J_{NN}$ coupling is much larger than the cis-$^2J_{NN}$ coupling. Interestingly, all cis-$^2J_{PN}$ and cis-$^2J_{NN}$ couplings measured in **1** were negative, while the trans-$^2J_{PN}$ and trans-$^2J_{NN}$ couplings were positive. The absolute signs of homonuclear and heteronuclear coupling constants have only been established for a limited number of organometallic complexes.[5,23,24] However, the same sign rule has been observed for the corresponding couplings between ^{1}H, ^{31}P, and ^{13}C spins in a number of octahedrally coordinated metal complexes (see, e.g. refs 4, 5, and 24). The present results show that couplings to ^{15}N, which has a negative gyromagnetic ratio, are no exception from this rule.

All the pulse sequences previously used for the analysis of coupling constants in tris(1-pyrazolyl)methane[8] were based on the HMQC experiment, which is insensitive to ^{1}H$-^1$H coupling evolutions during the relatively long constant delays needed to build up antiphase coherence with respect to the heteronuclear spins. When applied to **1**, however, the ^{1}H$-^1$H couplings that evolve during the evolution time obstructed the high resolution needed to resolve the additional multiplicity of the ^{15}N NMR signals due to small J_{PN} and additional J_{NN} couplings. Furthermore, the ^{1}H$-^1$H coupling evolution in the HMQC experiments resulted in mixed phases in the acquisition dimension of the spectra, calling for spectral representations in magnitude mode. The evolution of ^{1}H$-^1$H couplings in HMQC experiments can in principle be suppressed by the use of a ^{1}H spin-lock pulse during the evolution time.[25] However, experiments using this approach gave poor signal-to-noise ratios in our hands when using long evolution times for high-resolution spectra.

HSQC pulse sequences have several advantages over HMQC experiments: (1) HSQC experiments offer the possibility of applying spin-lock purge pulses[26,27] or pulsed field gradients[28] to select the desired heteronuclear antiphase magnetization and

(22) Otting, G. *J. Magn. Reson.* **1987**, *124*, 503−505.

(23) Pregosin, P. S.; Kunz, R. W. *NMR Basic Princ. Prog.* **1979**, *15*, 28, 34, and 86 and references therein. Verkade, J. G. *Coord. Chem. Rev.* **1972/73**, *9*, 1−106. Goodfellow, R. J.; Taylor, B. F. *J. Chem. Soc., Dalton Trans.* **1974**, 1676−1684. Pankowski, M.; Chodkiewicz, W.; Simonnin, M. *Inorg. Chem.* **1985**, *24*, 533−541. Hyde, E. M.; Kennedy, J. D.; Shaw, B. L.; McFarlane, W. *J. Chem. Soc., Dalton Trans.* **1977**, 1571−1576. Bowers, C. R.; Weitekamp, D. P. *J. Am. Chem. Soc.* **1987**, *109*, 5541−5542.

(24) Partridge, M. G.; Messerle, B. A.; Field, L. D. *Organometallics* **1995**, *14*, 3527−3530.

(25) Grzesiek, S.; Bax. A. *J. Biomol. NMR* **1995**, *6*, 335−339.

(26) Otting, G.; Wüthrich, K. *J. Magn. Reson.* **1988**, *76*, 569−574.

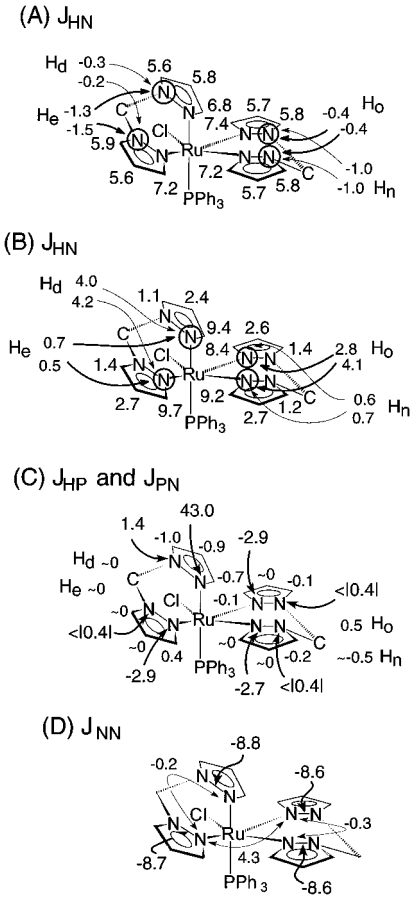

Figure 9. Overview over the coupling constants J_{HN} (A and B), J_{HP} and J_{PN} (C), and J_{NN} (D). In part A and B, only intra-pyrazolyl J_{HN} couplings with the circled ^{15}N spins are indicated. Furthermore, intra-bis-pyrazolyl J_{HN} couplings with the methylene protons are indicated, with arrows identifying the ^{15}N spin involved in the J_{HN} coupling. The values are plotted at the locations of the hydrogens involved in the J_{HN} couplings. No inter-bis-pyrazolyl J_{HN} coupling across the metal center could be resolved. In part C, the J_{HP} couplings with the single ^{31}P spin are indicated at the locations of the hydrogens involved. Arrows identify the ^{15}N spins involved in the J_{PN} couplings. In part D, single headed arrows identify $^1J_{NN}$ couplings. Double headed arrows identify $^2J_{NN}$ couplings. No inter-bis-pyrazolyl $^2J_{NN}$ or $^3J_{NN}$ couplings across the metal center other than the ones indicated in part D could be detected, placing upper bounds of |0.2| and |0.3| Hz, respectively, on these couplings. The uncertainties of the coupling constants are estimated to be less than 0.2 Hz. J_{CN} coupling constants of 12−14 Hz were measured for C_c/N_4, C_f/N_2, C_p/N_1, and C_m/N_3 with an accuracy of about 1 Hz. Similarly, J_{CN} couplings of 3−4 Hz were measured for C_b/N_4, C_g/N_2, C_q/N_1, and C_l/N_3. Isotope effects $\delta^{15}N(^{13}C) - \delta^{15}N(^{12}C)$ were >2 and <1 Hz for the one-bond and two-bond effects, respectively, for the C/N pairs for which J_{CN} couplings were measured.

suppress the t_1 noise from unwanted coherences. A single spin-lock purge pulse was sufficient to obtain clean spectra with **1**. (2) When a purging scheme by spin-lock pulses or pulsed field gradients with an HSQC experiment is used, the spectral quality is usually acceptable without additional coherence order selection by pulsed field gradients during the evolution time t_1. The recording of conventional phase-sensitive experiments improves the signal-to-noise ratio by $\sqrt{2}$ compared to experiments using coherence selection by pulsed field gradients during the evolution time. (3) For the long-range correlations needed with **1**, phase-sensitive spectra are automatically obtained with the HSQC experiments without the need for additional purging sequences.[29] (4) The HSQC experiments offer effective $^1H-^1H$ decoupling during t_1, since the ^1H spin terms are along the *z*-axis.[9] Exceptions occur when $^1H-^1H$ couplings evolve into antiphase magnetization during the INEPT delay and are converted into zero-quantum coherence by the second 90°(^1H) pulse.[27] Zero-quantum coherences evolve during t_1 under homonuclear $^1H-^1H$ coupling. Therefore, the spectra of **1** were recorded so that the large geminal J_{HH} coupling between the methylene protons was refocused by the end of the INEPT delay Δ. In this particular compound, the evolution of other $^1H-^1H$ couplings could be neglected, since they were all smaller than 3 Hz. For measurements of compounds with a larger spread of $^1H-^1H$ coupling constants, it may be advantageous to replace the 180°(^1H) refocusing pulse in the middle of the INEPT delay of the HSQC experiments by a selective 180°(^1H) refocusing pulse, which effectively decouples the set of refocused protons from all other protons. Clearly, the use of a selective 180°(^1H) pulse during the delay Δ would require the recording of different experiments with different frequencies of the selective 180°-(^1H) pulse to obtain cross peaks with all protons. Yet, this approach may well be worthwhile, since it not only improves the resolution in the F_1 dimension but also channels more ^1H magnetization into the desired coherence transfer pathway, resulting in enhanced sensitivity.

Several selective experiments do not necessarily require more time to record than a single nonselective experiment.[30] For example, eight different F_1-decoupled ^{15}N-HSQC experiments (Figure 5) were recorded here to determine the J_{PN} coupling with each of the eight individual ^{15}N resonances. Each of these selective experiments could be recorded in a very short time, since each spectrum contained the $^{15}N-^1H$ cross peaks with only a single ^{15}N resonance, allowing a very narrow spectral width in the F_1 dimension. Since the decoupling of the J_{NN} couplings improves the signal-to-noise ratio, the shortened experimental time per spectrum does not necessarily compromise the sensitivity compared to a nonselective experiment. In practice, it suffices to change the frequency of the selective 180°-(^{15}N) refocusing pulse (Figure 5) between the different experiments. Although this may lead to multiple folding of the signals in the F_1 dimension, the tilt of the E.COSY type multiplet pattern is unaffected when using the States−Haberkorn−Ruben[31] or States−TPPI[32] scheme for quadrature detection.

In principle, the relative signs of the small J_{NN} and J_{PN} couplings in **1** could also be determined by E.COSY type experiments. Since none of the protons in **1** is a common coupling partner for nitrogens located in different bis-pyrazolyl ligands and most J_{HP} couplings are below 1 Hz, it is not possible to correlate, e.g., N_6, N_7, and a proton, or N_7, P, and a proton in any simple ^1H-detected E.COSY type experiment. By using the mutually coupled spins N_6, N_7, and P, suitable E.COSY type $^{31}P-^{15}N$ or $^{15}N-^{15}N$ cross peaks could be generated, where the J_{NN} and J_{PN} couplings of interest appear as passive couplings. However, these experiments would necessarily be three-dimensional experiments, if ^1H detection is to be used for sensitivity enhancement. The DQ/ZQ-PN and DQ/ZQ-NN experiments yield the sign information of the J_{NN} and J_{PN} couplings in straightforward ^1H-detected two-dimensional experiments that are reasonably quick to record.

The experiments presented in this work produce antiphase multiplet fine structures in the acquisition dimension. The F_1-decoupled ^{15}N-HSQC experiment of Figure 5 and the LRNN

(27) Mattila, S.; Koskinen, A. M. P.; Otting, G. *J. Magn. Reson. B* **1995**, *109*, 326−328.
(28) Brühwiler, D.; Wagner, G. *J. Magn. Reson.* **1986**, *69*, 546−551.
(29) Mackin, G.; Shaka, A. J. *J. Magn. Reson. A* **1996**, *118*, 247−255.
(30) Cavanagh, J.; Waltho, J. P.; Keeler, J. *J. Magn. Reson.* **1987**, *74*, 386−393.
(31) States, D. J.; Haberkorn, R. A.; Ruben, D. J. *J. Magn. Reson.* **1982**, *48*, 286-292.
(32) Marion, D.; Ikura, M.; Tschudin, R.; Bax, A. *J. Magn. Reson.* **1989**, *85*, 393-399.

correlation and DQ/ZQ experiments of Figure 7 could be extended by a refocusing sequence $\Delta/2-180°(^1H,^{15}N)-\Delta/2$ and ^{15}N broadband decoupling during acquisition. This modification would improve the spectral resolution in the F_2 dimension, but the potential sensitivity gain achieved by decoupling would at least in part be compromised by relaxation and by the phase distortions arising from the evolution of J_{HH} couplings during the refocusing delay.

In principle, the appearance of the DQ/ZQ-NN experiment of Figure 8C could have been improved by decoupling the large homonuclear $^1J_{NN}$ couplings during t_1 by the use of a semiselective 180°(^{15}N) inversion pulse applied to N_1-N_4 in the middle of t_1 as in the DQ/ZQ-PN experiment of Figure 7B. However, the long selective pulse would have delayed the acquisition in the t_1 dimension, making a phase-sensitive recording difficult. The phase-sensitive representation of the DQ/ZQ-PN spectrum of Figure 8B was obtained by linear back-prediction of the first 21 points in the t_1 dimension. Yet, some artifactual peak intensity in the center of the J_{PN_8} multiplet of the ZQ cross peak was observed (Figure 8B). With a semiselective ^{15}N inversion pulse in the middle of t_1, many more data points would have had to be predicted for the DQ/ZQ-NN experiment of Figure 8C, because the increment in the t_1 dimension was much smaller.

Conclusions

Literature data on organometallic compounds show that the two-bond couplings between ^1H, ^{31}P, and ^{13}C spins across a metal center are commonly an order of magnitude larger, if the spins ligated to the metal are positioned trans rather than cis with respect to one another. The present data extend this result to $^2J_{PN}$ and $^2J_{NN}$ couplings. In addition to the magnitudes of the scalar couplings, the absolute sign of the scalar couplings was measured. The sign of the trans-$^2J_{PN}$ and trans-$^2J_{NN}$ couplings was found to be positive, while the sign of the corresponding cis couplings was negative. This, too, coincides with earlier results obtained for homo- and heteronuclear coupling constants measured between spins other than ^{15}N in a variety of different metal complexes, where the cis and trans couplings are opposite in sign. Although $^2J_{NN}$ couplings are significantly smaller than $^2J_{HP}$, $^2J_{PP}$, or $^2J_{PN}$ couplings, they are still readily measured and therefore a useful analytical tool for the conformational analysis of organometallic complexes. In summary, $^2J^{15}_{N-Ru-X(cis)} < 0$; $^2J^{15}_{N-Ru-X(trans)} > 0$; $|^2J^{15}_{N-Ru-X(trans)}| \gg |^2J^{15}_{N-Ru-X(cis)}|$, X = ^{31}P, ^{15}N.

The measurement of the heteronuclear coupling constants in organometallic compounds is in several aspects less straightforward than the measurement of small couplings such as those found in proteins because of the vast range of different ligands and ligand configurations possible, which represent quite different spin systems. Yet, many of the ideas adapted here for the use with organometallic molecules were originally developed for applications with peptides and proteins. Examples are the F_1 decoupling by a combination of a soft pulse with a hard pulse,[19] the encoding of coupling constants in relative cross peak intensities,[20] and the comparison of double-quantum and zero-quantum cross peaks.[21,22] It may be anticipated that further multinuclear experiments originally developed for biomolecular NMR can be adapted to the analysis of small molecules.

Experimental Section

Synthesis of Chloro(triphenylphosphine)bis[bis(1-pyrazolyl)-methane]ruthenium(II) Chloride, $[RuCl(PPh_3)(BPM)_2]^+Cl^-$ (1). The 99% ^{15}N-labeled ligand bis(1-pyrazolyl)methane was synthesized with use of 99% ^{15}N-labeled hydrazine sulfate.[8,33] The 99% ^{15}N-labeled metal complex **1** was synthesized from 99% ^{15}N-labeled bis(1-pyrazolyl)methane and $RuCl_2(PPh_3)_3$,[34] following a previously described method.[7]

NMR chemical shifts: ^1H (400 MHz; solvent CD_3OD, referenced against residual solvent ^1H signal as 3.50 ppm): δ 8.46 [H_r], 8.43 [H_c], 8.25 [H_f], 8.23 [H_e], 8.21 [H_p], 8.17 [H_m], 7.55−7.21 [aromatics], 7.54 [H_a], 6.99 [H_d], 6.74 [H_q], 6.69 [H_o], 6.52 [H_b], 6.47 [H_l], 6.41 [H_g], 6.04 [H_k], 5.86 [H_h], 5.72 [H_n]. ^{13}C (100 MHz, solvent CD_3OD, referenced against the solvent ^{13}C resonance as 49.3 ppm): δ 151.6 [C_a], 148.8 [C_r], 147.1 [C_k], 144.2 [C_h], 137.0 [C_c], 136.4 [C_m], 136.0 [C_p], 134.6 [C_f], 134.6−128.8 [PPh_3], 110.0 [C_l], 109.4 [C_q], 109.1 [C_b], 108.9 [C_g], 64.3 [$C_{d,e}$], 63.4 [$C_{o,n}$]. ^{15}N (60 MHz; solvent CD_3OD, referenced against external nitromethane): δ −170.13 [N_1], −167.90 [N_2], −167.34 [N_3], −163.51 [N_4], −153.70 [N_5], −151.15 [N_6], −149.40 [N_7], −128.21 [N_8]. ^{31}P (162 MHz, solvent CD_3OD, referenced against external neat trimethyl phosphite taken as 140.85 ppm): δ 49.3.

Two-Dimensional NMR Experiments. The semiselective ^{15}N inversion pulse applied in the middle of the INEPT delay in any of the experiments described here was a hyperbolic secant pulse[35] of 12.5-ms duration. This pulse was suitable for the simultaneous selective inversion of N_1, N_2, N_3, and N_4. While the ^{15}N resonances of N_5, N_6, and N_7 were close to each other in frequency, the resonance of N_8 was further separated. To obtain good simultaneous inversion of N_5 to N_8 without affecting the resonances N_1 to N_4, a 12.5-ms hyperbolic secant pulse was used, which was modulated by a cosine function to produce two simultaneous excitation ranges, one centered on the resonances N_5 to N_7 and the other on the frequency of N_8. This pulse was applied with an offset placing its effective frequency half-way between the ^{15}N frequencies of N_5 to N_7, and N_8. With the exception of the DQ/ZQ experiments, quadrature detection in the indirect frequency dimension was achieved by incrementing the phases of all ^{15}N or ^{13}C pulses preceding the evolution time t_1 in the States−TPPI[32] manner. The DQ/ZQ experiments were recorded without quadrature detection in the F_1 dimension. Instead, the carrier frequencies were placed at the high-field end and the t_1 data Fourier transformed with a cosine FT. The spectral representations in Figure 8 were obtained by setting the reverse flag for the F_1 dimension in the processing software of the spectrometer manufacturer (xwin-nmr1.2). Before Fourier transformation, the data were multiplied by a cosine window function in both dimensions. To alleviate the linebroadening effect of the window multiplication in the F_1 dimension, the t_1 data were extended by linear prediction with use of the algorithm provided in xwin-nmr.

Acknowledgment. The authors thank Bruker for the generous loan of a $^1H/^{31}P/^{13}C/^{15}N$ probehead which was used for the DQ/ZQ experiments. G.O. thanks the Swedish Natural Science Research Council (Project 10161) and the Knut och Alice Wallenberg foundation for financial support. B.A.M. and L.P.S. thank the Australian Research Council for support and the University of Sydney for a Gritton Scholarship.

JA963346B

(33) Julia, S.; del Mazo, J. M.; Avila, L.; Elguero, J. *Org. Prep. Proced. Int.* **1984**, *16*, 299−307.

(34) Stephenson, T. A.; Wilkinson, G. *J. Inorg. Nucl. Chem.* **1966**, *28*, 945−956.

(35) Silver, M. S.; Joseph, R. I.; Hoult, D. I. *J. Magn. Reson.* **1984**, *59*, 347−351.